



Field observation of the wave-induced pore pressure response in a silty soil seabed

Xingbei Xu¹ · Guohui Xu¹ · Junjie Yang¹ · Zhongqian Xu² · Yupeng Ren¹

Received: 7 June 2020 / Accepted: 14 December 2020 / Published online: 4 February 2021
© The Author(s), under exclusive licence to Springer-Verlag GmbH, DE part of Springer Nature 2021

Abstract

Liquefaction of seabed sediments under the action of storm waves is an important form of seabed instability, which may cause damage to submarine structures such as pipelines and cables. A commonly used parameter to identify sediment liquefaction is pore pressure. The pressure response of the pore water at different depths of a silty soil seabed under storm waves was monitored by a probe rod in the Yellow River delta. The probe is made of a steel pipe with a length of 8 m and an outer diameter of 10 cm, which is equipped with 10 pore pressure sensors. According to the collected data, under a water depth of 8 m, silty soil seabed liquefaction starts when the significant wave height reaches 0.5 m, and the liquefaction depth is between 3.3 and 3.8 m under waves with a significant wave height of 3.65 m. Seabed liquefaction develops in a top-down manner, and the average development rate of the liquefaction depth is approximately 0.17 m/min.

Keywords Wave-induced liquefaction · Pore pressure · Field observation · Silty soil seabed

Introduction

Under the action of storm waves, seabed sediments can become unstable, and seabed liquefaction caused by strong dynamic action is an important form of seabed instability. Together with erosive processes and cyclic loads on infrastructure, seabed liquefaction represents a serious threat to the safety of seabed structures. Wave-induced liquefaction can be divided into two cases according to different mechanisms of generation: (1) residual liquefaction caused by a buildup of pore pressure (residual excess pore pressure) and (2) momentary liquefaction caused by an upward directed vertical pressure gradient (oscillatory excess pore pressure) in the soil during the passage of a wave trough (Sumer 2014). A steel pipeline with a diameter of 3.05 m buried under Lake Ontario has been fractured many times during severe storms, and the damage is believed to be caused by the liquefaction of backfill (Christian et al. 1974). In 2003, submarine cables in the Chengdao Oilfield were

interrupted after storms, and a sub-bottom profile indicated that a disturbance zone in the seabed extends to a depth of 4 m; this disturbance zone probably formed due to liquefaction of the seabed under wave action (Xu et al. 2009). In addition, according to field investigations, sediment collapse craters are widely distributed on the seabed, ranging from ten to hundreds of meters in diameter and up to 5 m in depth (Prior et al. 1986; Chen et al. 1992). Laboratory tests indicate that these sediment collapse craters are most likely formed due to the liquefaction-induced seabed compaction and material transport (Sumer et al. 2006a; Xu et al. 2016b).

The responses of seabed sediments to dynamic actions such as waves and seisms can reflect their stability, and as an important consideration of the geotechnical properties of sediments, pore pressure has long played a role in the field monitoring of sediment responses under strong dynamic conditions (Richards et al. 1975; Bennett 1977; Davis et al. 1991). Due to the limitation of factors such as the contingency and complexity of field monitoring, many studies have been carried out through laboratory experiments (Zen and Yamazaki 1990a; Sassa and Sekiguchi 1999; Sumer et al. 2006a; Kirca et al. 2013) and numerical simulations (Dalrymple and Liu 1978; Liu et al. 2010; Cha et al. 2011; Gagniere et al. 2018; Qi and Gao 2018), which provide a better understanding of the pore pressure response during seabed liquefaction and the mechanisms of wave-induced seabed liquefaction. However, field monitoring

✉ Guohui Xu
xuguohui@ouc.edu.cn

¹ College of Environmental Science and Engineering, Ocean University of China, Qingdao 266100, People's Republic of China

² Services Authority of Qingdao International Cruise Port Zone, Qingdao 266005, People's Republic of China

is still an important means of studying seabed liquefaction and can not only verify the accuracy of laboratory results but also provide valuable reference data for numerical simulations.

Currently, field monitoring of liquefaction is focused primarily on sandy seabeds. Zen and Yamazaki (1991) monitored the periodic response of the pore pressure in a sandy seabed under the cyclic loading of waves with a water depth of 4–6 m and found that the liquefaction depth of the seabed was approximately 39 cm (between 22 and 69 cm) when the pressure fluctuation amplitude at the seafloor was 8.81 kPa. By embedding pore pressure sensors at different depths of the seabed, Sassa et al. (2006) monitored the accumulation and dissipation of the pore pressure in sediments under a water depth of 15 m during a typhoon, and the data show that the pore pressure begins to increase when the wave height exceeds 2 m, while the liquefaction depth reaches 10 cm when the wave height exceeds 4 m. Mory et al. (2007) monitored pore pressure in situ and found that there was no increase in residual pore pressure in the seabed and that momentary liquefaction of the seabed occurred under wave action: the liquefaction depth reached 30 cm when the significant wave height reached 0.5–0.9 m for a seabed under a water depth of 2 m. Silty soil is widely distributed in various estuarine regions of the world, such as the Yellow River delta and Mississippi Delta (Bornhold et al. 1986; Williams et al. 2006). However, the liquefaction of silty seabeds under wave action lacks evidence in the form of direct field data. Bennett and Faris (1979) detected the rise in seabed pore pressure under the action of storms in the Mississippi Delta and regarded the pressure increase as a result of undissolved gas without connecting it to liquefaction of the seabed. During a field survey of the Yellow River delta region, Prior et al. (1989) found that a seabed-monitoring instrument sank into the sediment during a storm, accompanied by a pore pressure rise, but the hypothesis of seabed liquefaction was not confirmed. According to calculations, Puzrin et al. (2010) determined that the silty ground of a caisson of a breakwater in Barcelona had been liquefied under the action of strong waves, but the development process of liquefaction remained unknown.

In this study, the pore pressure response of a silty soil seabed under the action of strong waves was monitored by a probe in the Yellow River delta region. Residual liquefaction of the silty soil seabed was identified according to the collected pore pressure data, and the speed of the development of silty soil seabed liquefaction under wave action was also revealed.

Field monitoring and data processing

Observation site

The site monitoring point is located in the Chengdao area of the Yellow River delta (Fig. 1). The water depth is 8.4 m, and

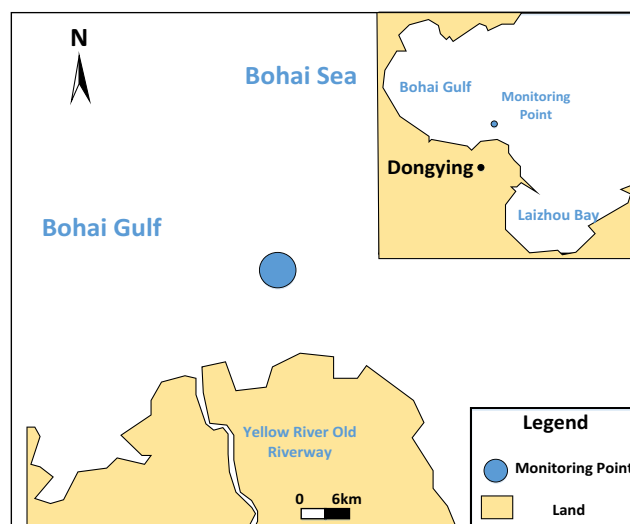


Fig. 1 Monitoring site

borehole data near the monitoring site show that the seabed sediments here are silty soil (0–3 m), silty sand (3–3.5 m), muddy silty clay (3.5–4.2 m), and silty soil (4.2–7.8 m), from top to bottom. The characteristics of the soil are shown in Table 1.

The monitoring method relied on embedding probes in the seabed by first drilling a borehole with a slightly smaller diameter (0.094 m) and then pressing the probe into the borehole. According to the response of the excess pore pressure, the disturbance caused by the insertion of the probe gradually disappeared within 17 h after the instrument was installed (“Excess pore pressure”). The probe is made of a steel pipe with a length of 8 m and an outer diameter of 10 cm. The 86-030G-C piezo resistive pressure IC sensors were used in the monitoring. The sensor has a diameter of 2 cm and a length of 5.3 cm. The accuracy of the sensor is 0.2% FS. The burial depths of the pore pressure sensors in the seabed were 0.3, 0.8, 1.3, 1.8, 2.3, 2.8, 3.3, 3.8, and 4.8 m. One pore pressure sensor was set to monitor the pressure response at 0.2 m above the seafloor. A data acquisition, data storage, and power supply device fixed on a pile was placed near the monitoring point to provide power for the pore pressure sensor and automatically collect and store the pore pressure sensor data according to the preinstalled program. The layout of the field data monitoring system is shown in Fig. 2.

The acquisition system recorded 1-min data at a sampling frequency of 50 Hz every 9 min after installation at 16:00 on 4 November 2015.

Data analysis method

The pore pressure data are acquired by correcting the initial collected data using the calibration equation provided by the manufacturer.

Table 1 Basic parameters of soil properties of field observation

	d (mm)	W_g (%)		γ (kN/m ³)		K (cm/s)	
	Average	Range	Average	Range	Average	Range	Average
Silty (0–3.0 m, 4.2–7.8 m)	0.063	22.32–24.55	24.18	19.21–19.82	19.42	1.15×10^{-5} – 1.72×10^{-5}	1.67×10^{-5}
Muddy silty clay (3.5–4.2 m)	0.004	30.91–43.80	39.42	17.82–18.67	18.34	1.21×10^{-6} – 1.91×10^{-6}	1.43×10^{-6}
Silty sand (3.0–3.5 m)	0.097	17.18–18.97	17.91	19.43–20.12	19.82	6.13×10^{-4} – 7.57×10^{-4}	6.32×10^{-4}

Reference standards: <the engineering classification standard of soil>, China, GB/T 50145–2007); <code for investigation of geotechnical engineering>, China, GB 50021–2001)

Wave characteristics

During the field observations of Zen and Yamazaki (1991), it was found that although the high-frequency components of the water surface could not be represented, the dynamic response of the monitored seabed was basically the same as that of the waves. Thus, the wave conditions in the field can be judged by the pore pressure sensor located above the seafloor on the pile. The pressure difference and wave period during the monitoring period were read from the recorded data using the zero-up-crossing method (as shown in Fig. 3). While using this method, it is necessary to obtain the reference line, i.e., the water depth during the monitoring period. Due to the

influence of tides, the water depth of each monitoring period at the monitoring point is not a fixed value. During data processing, water depth h is calculated every 10 min by averaging the 1-min monitoring data of sensor no. 10 in water. This water depth is also used in the calculation of static pore pressure.

According to small-amplitude wave theory, the relationship between the pressure difference P and wave height H is approximately

$$P = K_p \rho g H \tag{1}$$

where K_p is the pressure coefficient. If the pressure is recorded at the water-seabed interface with a water depth of h , K_p can be calculated by

$$K_p = \frac{1}{\cosh(kh)} \tag{2}$$

where $k = 2\pi/L$ and can be solved from the dispersion relation

$$\omega^2 = gk \tanh(kh) \tag{3}$$

with $\omega = 2\pi/T$.

By combining Eqs. (1), (2), and (3), H can be calculated.

Wave heights in a wave train obey the Rayleigh distribution. Although the data recorded in the field were not

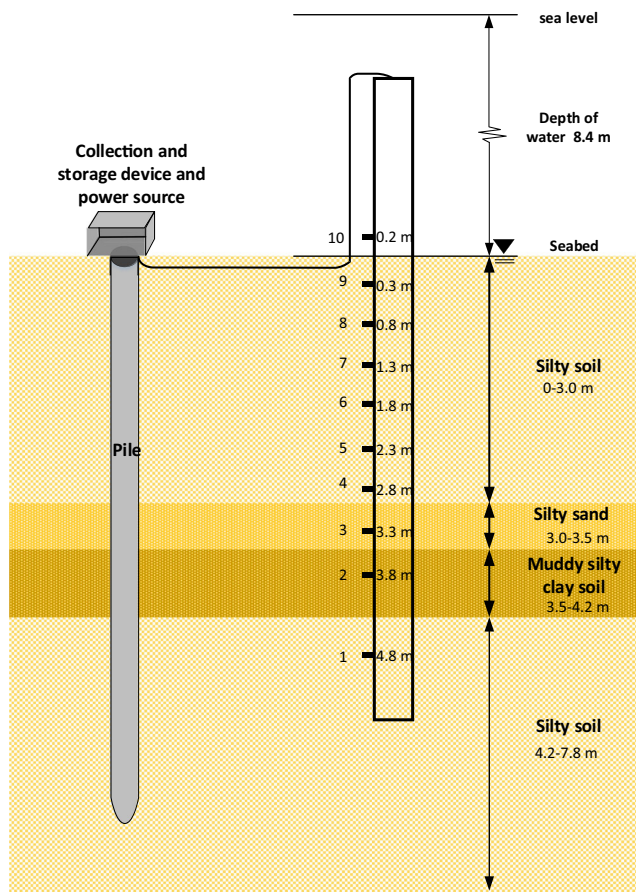


Fig. 2 Arrangement of sensors in monitoring point

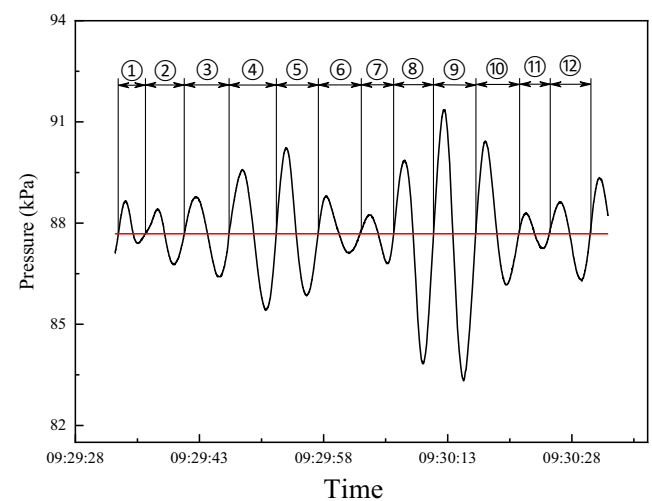


Fig. 3 Monitoring data of pressure sensor no. 10

continuous, since they represent data randomly taken from the wave train, the wave heights should still obey the Rayleigh distribution. Thus, the statistical characteristics of the wave parameters were calculated using empirical equations. The significant wave height is

$$H_{1/3} \approx 1.6\bar{H} \quad (4)$$

where \bar{H} is the average height. The significant wave period is

$$T_{1/3} \approx 1.1\bar{T} \quad (5)$$

where \bar{T} is the average period.

Excess pore pressure

Under the wave load, the increase in excess pore pressure is an important index to indicate the change in soil state. The change in excess pore pressure can be used to judge whether the field soil state is liquefaction or not.

The static pore pressure at a certain depth is calculated as

$$P_0 = \gamma_w(h + z) \quad (6)$$

where P_0 is the static pore pressure, kPa; γ_w is the unit weight of the sea water, kN/m³; h is the water depth, m; and z is the burial depth of the sensor, m.

Then, the excess pore pressure is

$$P_e = P_m - P_0 \quad (7)$$

where P_e is the excess pore pressure, kPa, and P_m is the measured pore pressure, kPa.

The residual excess pore pressure is

$$\bar{P}_e = \bar{P}_m - P_0 \quad (8)$$

where \bar{P}_e is the residual excess pore pressure, kPa, and \bar{P}_m is the measured period-averaged pore pressure, kPa.

Taking sensor no. 10 as the reference sensor, based on the relative position of each other sensor, the changes in residual excess pore pressure in each layer of the site were calculated according to the above equation.

Effective stress

The effective stress of the soil reflects the soil stability. The response of the excess pore pressure in sediments will influence the effective stress, thus leading to a change in sediment stability.

The vertical effective stress of soil under static water conditions is

$$\sigma_{v0}' = (\gamma_s - \gamma_w) \cdot z \quad (9)$$

where γ_s is the effective unit weight of the soil, kN/m³.

The initial mean normal effective stress of the soil under static water conditions is

$$\sigma_0' = \frac{1 + 2k_0}{3} (\gamma_s - \gamma_w) \cdot z \quad (10)$$

where k_0 is the lateral earth pressure coefficient at rest, which is taken as 0.5 in this paper.

Under a cyclic wave load, the pore pressure in the soil will increase and induce excess pore pressure P_e , and the effective stress σ_v' will decrease with increasing excess pore pressure:

$$\sigma_v' = \sigma_{v0}' - P_e \quad (11)$$

It is widely accepted that when the effective stress is reduced to 0 or when the pore pressure reaches the initial mean normal effective stress, liquefaction occurs. Thus, P_e/σ_{v0}' (Zen and Yamazaki 1990b) and \bar{P}_e/σ_0' (Kirca et al. 2013) can be used to reflect liquefaction. A closer value of P_e/σ_{v0}' or \bar{P}_e/σ_0' to 1 corresponds to more unstable soil. Both metrics are used in the identification of seabed liquefaction. The liquefaction time of each layer is determined by evaluating when the P_e/σ_{v0}' or \bar{P}_e/σ_0' reaches 100%.

Observation results

According to meteorological data (Table 2), there were strong winds and waves in the monitoring area during 4–7 November 2015, which may have led to instability of the seabed. The wave height increased from less than 1 m to more than 4 m on 5 November, so the monitoring data in this period were analyzed in detail. At the very beginning of the wave height increase (8:29–8:49), the field monitoring data were not recorded, and the reason for this issue remains unknown.

Wave characteristics

Using the data collected by the pore sensor 0.2 m above the seafloor (sensor no. 10), the wave characteristics on 5 November were obtained by the method described in “Wave characteristics” section, and the results are shown in Fig. 4.

As shown in Fig. 4a, the waves at the monitoring site were small before 9:00, with $H_{1/3}=0.3$ m. Then, the wave height

Table 2 Weather forecast of 4–6 November 2015 (the Yellow River delta)

Date	Direction and wind intensity (m/s) (day/night)
4 November 2015	South 5–7/South 5–7
5 November 2015	Northeast 5–9/Northeast 9–12
6 November 2015	Northeast 9–12/Northeast 9–12

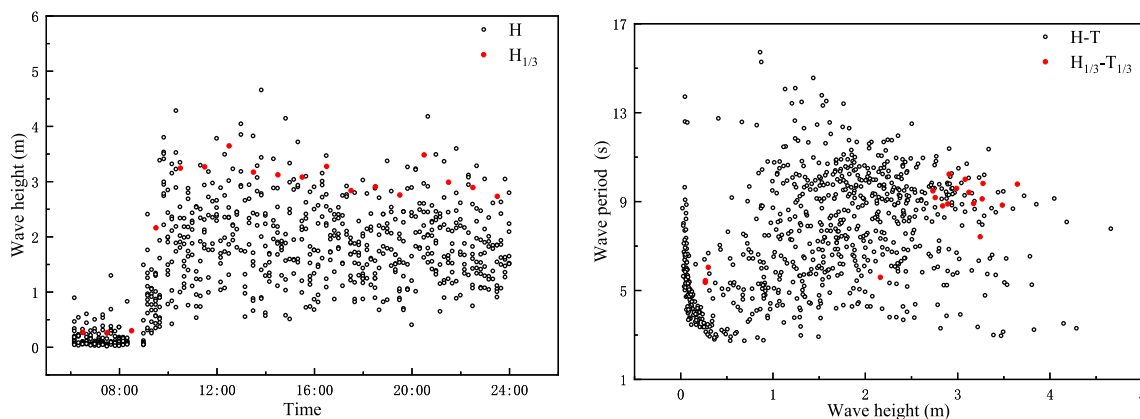


Fig. 4 Wave characteristics on 5 November. **a** Time distribution of H and $H_{1/3}$. **b** $H-T$ and $H_{1/3}-T_{1/3}$

gradually increased, and $H_{1/3}$ peaked at 3.65 m at approximately 12:30. Figure 4 b shows the relationship between $H - T$ and $H_{1/3} - T_{1/3}$. When $H_{1/3}$ was at least 2.5 m, $T_{1/3}$ fluctuated for approximately 9 s, which is probably related to the fragmentation of the high waves passing through the monitoring area (Zen and Yamazaki 1991). In addition, wave groups were detected during the observation period (Fig. 5). As the red dotted box shows in Fig. 5, waves with small wave heights and long periods will appear near the junction point of the two wave groups.

Pore pressure

The periodical average pore pressure recorded at each layer linearly increases with depth before the increase in wave height, which indicates that the sensors are in good working condition. According to Fig. 4, the load acting on the soils changed notably between 7:00 and 11:00, increasing from small ($H_{1/3} = 0.27$ m) to large waves ($H_{1/3} = 3.27$ m), and the pore pressure response changed significantly (refer to Fig. 6). Affected by the tide, the pore pressure of each layer increases from 7:40 to 9:00, but the relative value remains unchanged; in addition, the

oscillation amplitude increases at 9:00 due to the larger wave. In contrast, the pore pressure behaves much differently after 9:00: except for the difference caused by water level changes due to the tidal action (refer to the change in periodical average pore pressure at the seafloor), the periodical average pore pressure significantly increased from 0.8 to 3.3 m. The irregular response of sensor no. 9 (0.3 m burial depth) to the wave action suggests that this sensor may have been damaged during the deployment of the monitoring equipment, so the data collected by it are not presented in the following analysis.

The response of the pore pressure to waves is attenuated with depth, and the attenuation is closely related to the composition and state of the seabed sediments. The relative pore pressure response of each layer can be expressed by P_z/P , where P is the variation range of the pressure at the seafloor and P_z is the variation range of the pore pressure at burial depth z . The pressure oscillation near the seafloor is represented by the value of sensor no. 10. The relative pore pressure response of each layer in the process of wave enlargement is plotted in Fig. 7.

As shown in Fig. 7, the relative pore pressure response tends to decrease gradually with depth. With the gradual increase in wave height, the relative pore pressure response of

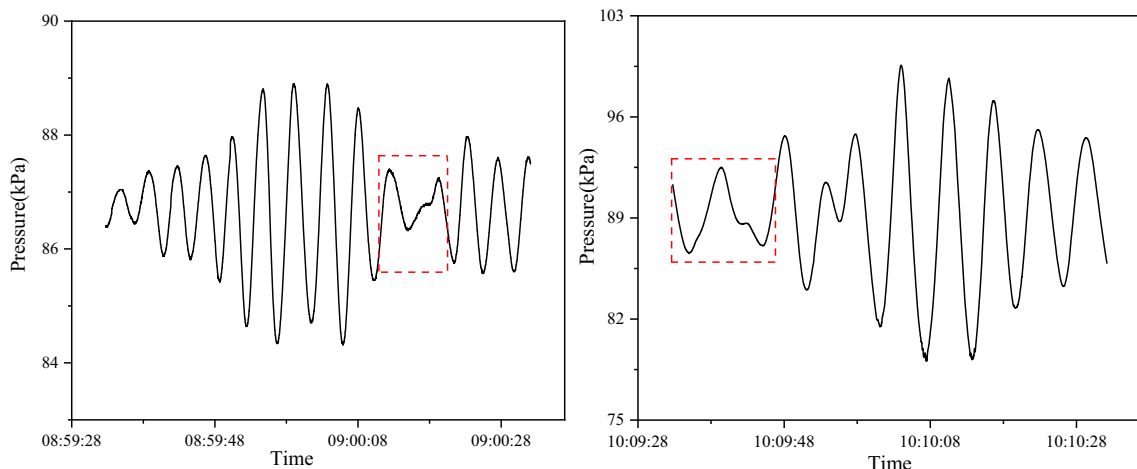
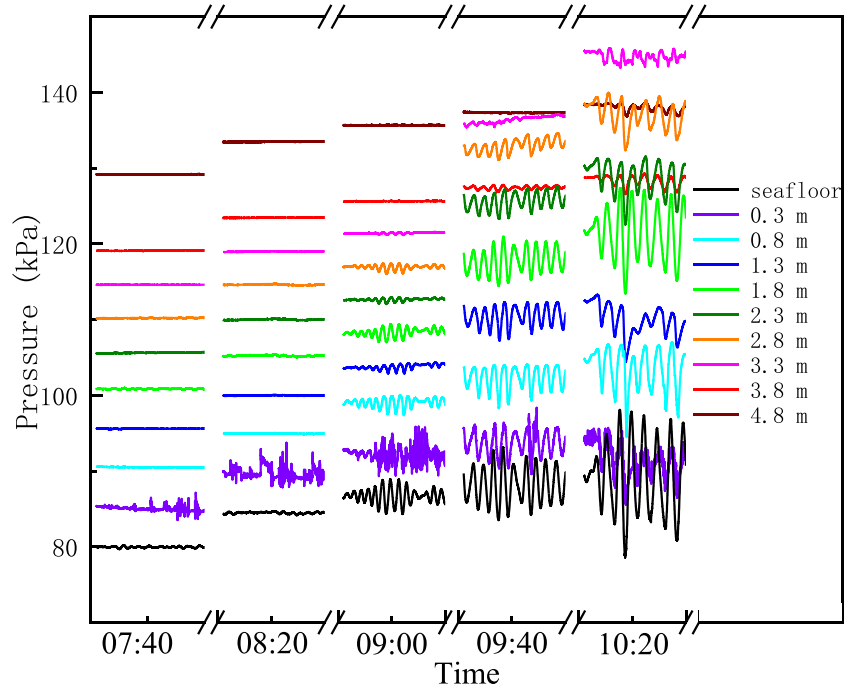


Fig. 5 Wave group monitored by sensor no. 10

Fig. 6 Time-history curve of pore pressure during increase of wave height



each layer increases gradually with depth. Compared with 8:59, the relative pore pressure response of each layer increases notably at 10:09. However, the variation trends of the pore pressure at depths of 0.8 m and 1.3 m are not distinct. The time-history curves of the pore pressure in these two layers are plotted in Fig. 8.

The pore pressure at depths of 0.8 m and 1.3 m responds well to small waves (Fig. 8a), but anomalous pore pressure responses are observed as the wave height increases (Fig. 8 b, c, and d). These anomalies lead to a deviation in the relative pore pressure responses of these layers from the normal values.

Excess pore pressure

Based on the position of the no. 10 sensor in the seawater and the relative positioning of each other sensor, the change in residual excess pore pressure in each layer was calculated according to Eq. (8) (see Fig. 9).

Due to the slightly larger diameter of the monitoring probe, excess pore pressure is generated during insertion of the probe, and the greater the depth is, the higher the induced excess pore pressure. Then, the excess pore pressure begins to dissipate gradually from bottom to top, reaching

Fig. 7 Relative pore pressure responses of different layers

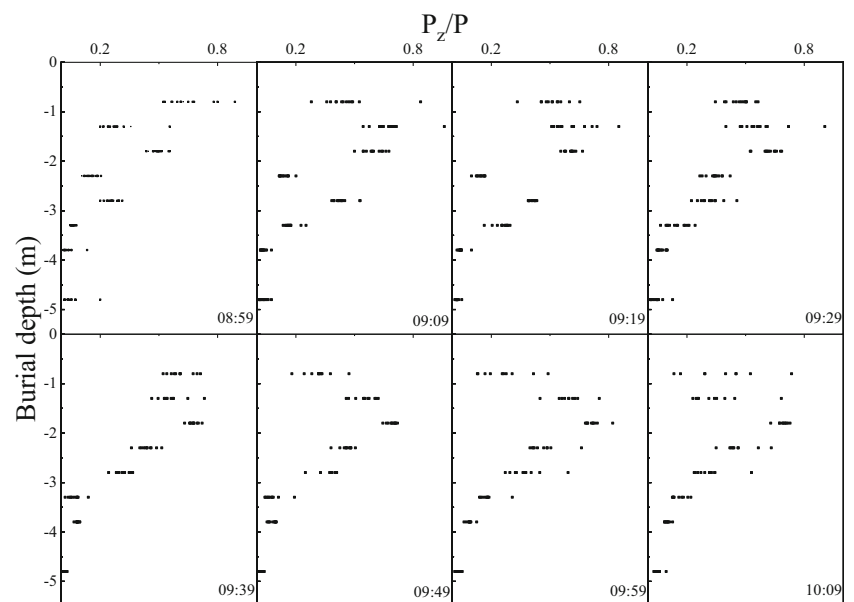
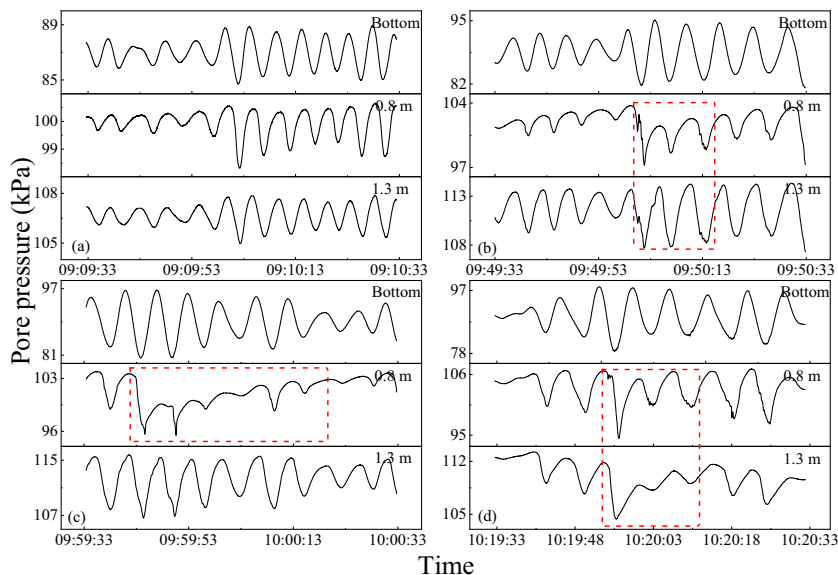


Fig. 8 Time history curves of pore pressure response at depths of 0.8 m and 1.3 m



approximately 0 kPa at 8:00 on 5 November. Therefore, the disturbance of the seabed caused by the equipment layout has been basically eliminated.

When the wave intensity increases, the excess pore pressure in the seabed notably changes: in the layers from 0.8 to 3.3 m, the excess pore pressure increases from shallow to deep, and the deeper the depth is, the greater the residual

excess pore pressure; however, almost no excess pore pressure was observed in the 3.8-m and 4.8-m layers. At approximately 10:00, the excess pore pressure at a depth of 3.3 m reaches the maximum value. At depths deeper than 3.8 m, although the excess pore pressure fluctuates, no residual excess pore pressure was observed. After the excess pore pressure peaks, the excess pore pressure gradually decreases from deep to shallow

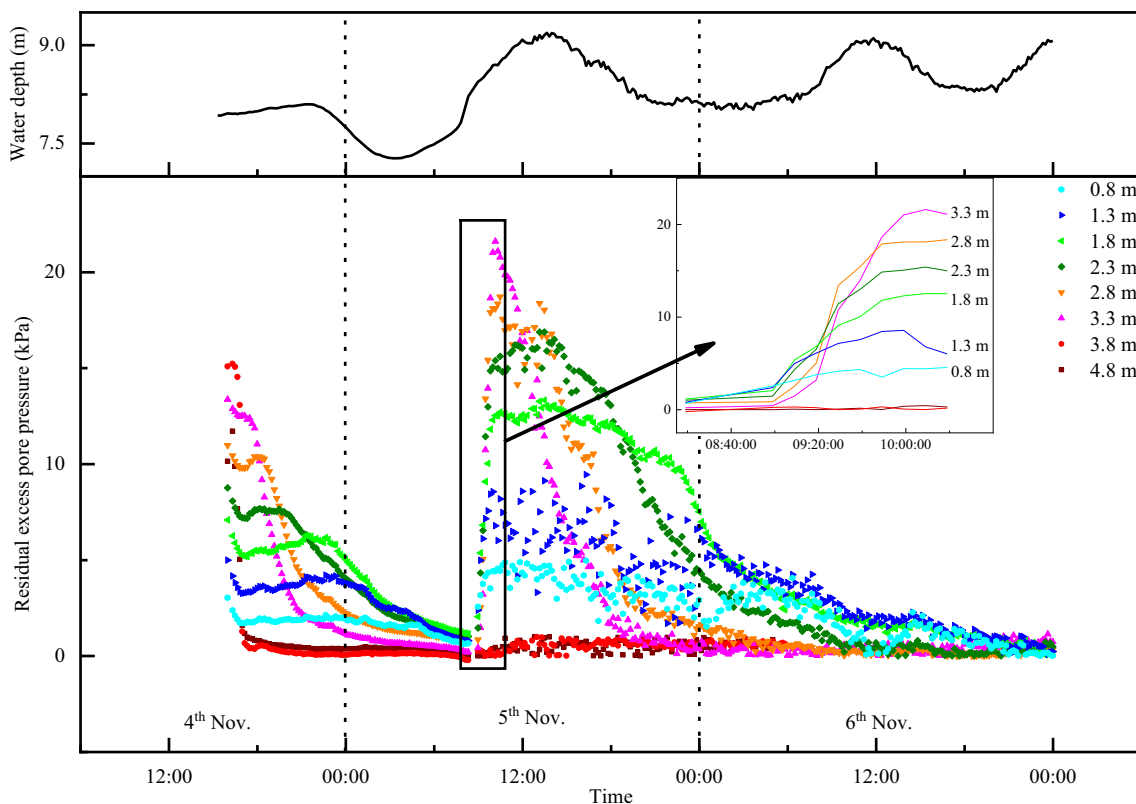


Fig. 9 Time history curve of residual excess pore pressure in situ

and approaches the excess pore pressure observed before the strong wave action at the end of 6 November (the sensor data at 3.8 and 4.8 m were missing after 5:59 and 5:29 on 6 November, respectively). During this process, the wave height does not decrease, which is consistent with the results of indoor wave flume experiments (Sumer et al. 2006a). This can be explained by the restructuring and solidification of the sediment (Miyamoto et al. 2004; Xu et al. 2016a). The restructured sediment shows a characterization of increasing strength, density, median particle size, and reducing water content and clay content (Wang et al. 2017). The wave action cannot maintain the liquefaction of sediment, and excess pore pressure gradually dissipates under the upward-directed pressure gradient.

The oscillatory excess pore pressure response under the action of the maximum wave height of each data segment during the increase in residual excess pore pressure was selected for analysis. As shown in Fig. 10, the phases of the waveforms of the excess pore pressure and waves are inversely related, i.e., P_e reaches its minimum value at the wave crest and its maximum value at the wave trough. This phenomenon is consistent with the phenomena observed by Zen and Yamazaki (1991). According to Eq. (11), the vertical effective stress reaches its minimum value at the wave trough, which means that the seabed is more prone to liquefaction. Thus, the pore pressure used in the identification of liquefaction with P_e/σ'_{v0} is taken from the wave trough.

Effective stress

According to the change in excess pore pressure, the effective stress of the soil from 9:00 to 10:30 during field monitoring was calculated by Eq. (11), and the change process of the effective soil stress under cyclic wave loading was obtained (Fig. 11; Tables 3 and 4).

According to Fig. 11, a significant reduction occurred in the effective soil stress at depths from 0.8 to 3.3 m when the wave changed from small waves at 8:00 ($H_{\max}=0.16$ m) to large waves at 10:10 ($H_{\max}=3.43$ m), while the change was slight at depths of 3.8 m and 4.8 m. At the same time, for the sediment at depths from 0.8 to 3.3 m, P_e/σ'_{v0} changed from less than 10% to more than 93%, and \bar{P}_e/σ'_{v0} changed from less than 20% to more than 100%, while these metrics remained almost unchanged (less than 22.3% for P_e/σ'_{v0} and less than 4.2 for \bar{P}_e/σ'_{v0}) at the depths of 3.8 m and 4.8 m.

Discussion

Occurrence of liquefaction

The increase in excess pore pressure is caused by the displacement of particles in seabed sediments under wave loading, and laboratory experiments indicate that displacement occurs

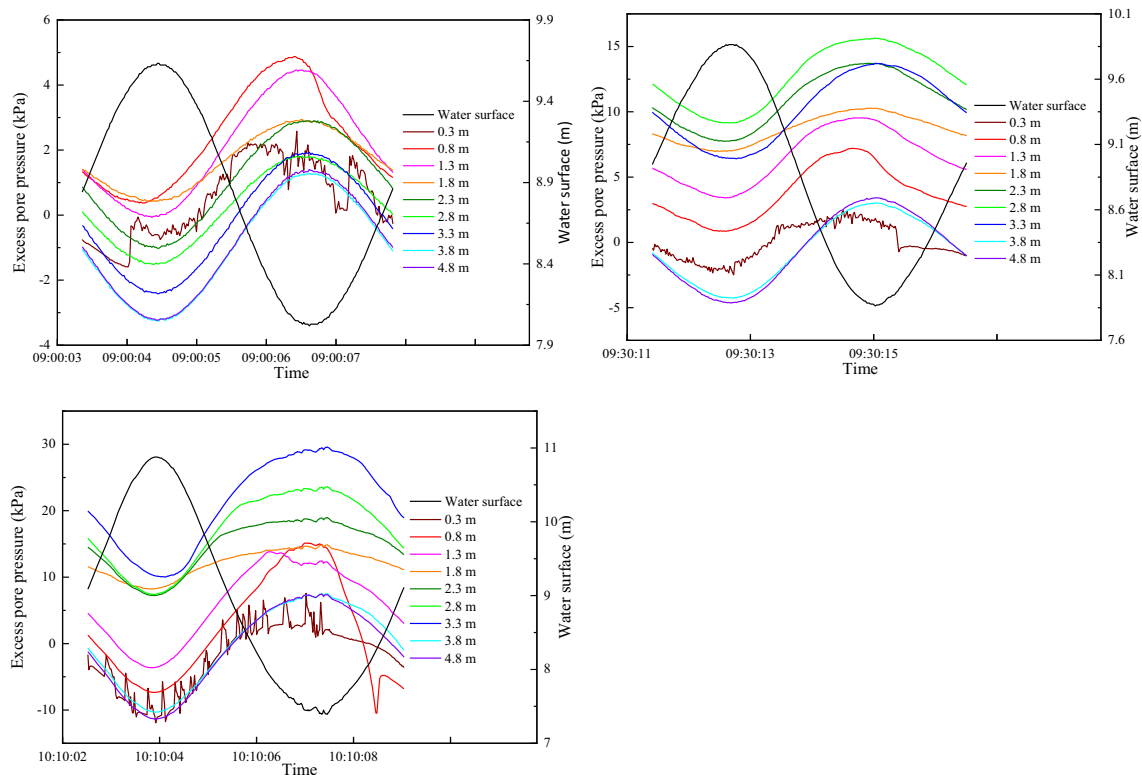
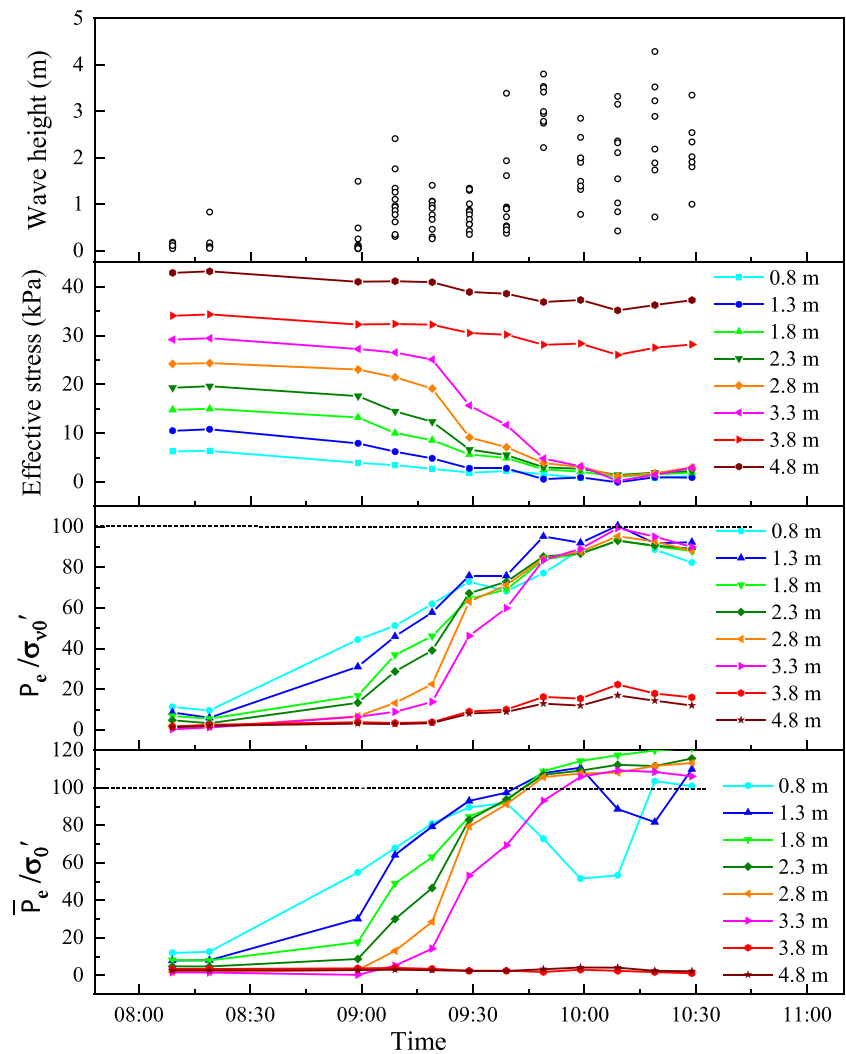


Fig. 10 Time-history curves of oscillatory excess pore pressure under the maximum wave height in a data segment

Fig. 11 Time history curve of wave height and effective stress



more easily when structures such as pipelines are present (Sumer et al. 2006b).

Table 3 The ratio of p_e/σ_{v0}' in each layer

Time	p_e/σ_{v0}' (%)							
	0.8 m	1.3 m	1.8 m	2.3 m	2.8 m	3.3 m	3.8 m	4.8 m
8:19	9.6	5.9	5.5	3.2	1.4	1.2	2.4	2.0
8:59	44.4	31.0	16.8	13.3	6.7	6.4	3.8	3.1
9:09	51.2	46.0	36.8	28.7	13.2	8.9	3.4	2.8
9:19	61.9	57.7	46.1	39.0	22.5	13.8	3.8	3.3
9:29	72.9	75.8	64.4	67.2	63.0	46.2	8.9	8.0
9:39	68.2	75.8	69.0	72.9	71.2	59.9	10.0	8.8
9:49	77.1	95.1	83.7	85.2	84.3	83.5	16.1	12.9
9:59	88.6	92.0	86.7	86.7	87.6	89.0	15.4	11.9
10:09	87.9	100.4	93.2	93.0	95.2	99.2	22.3	17.0
10:19	88.6	91.7	90.3	90.7	92.6	95.0	17.9	14.3
10:29	82.3	92.3	87.9	89.0	88.0	90.0	15.9	11.9

The time-history curves of the excess pore pressure in each layer from 0.3 to 3.3 m as the wave height increases (8:00–10:30) are shown in Fig. 12. Similar to previous laboratory experimental results (Sumer et al. 2006a; Sumer et al. 2006b), the liquefaction process of the soil in a certain layer goes through three stages: the excess pore pressure ① begins to increase, ② rapidly increases, and ③ reaches the maximum value. The increase in excess pore pressure will cause a decrease in the effective stress in the seabed, which leads to liquefaction. Thus, stage ① reflects the characteristics required to predict the start of residual liquefaction under continuous wave action. For the layer at depths 3.8 m and 4.8 m, although there is an increase in transient excess pore pressure, which is consistent with that in the shallower layer, the residual excess pore pressure remains almost unchanged. The increase in transient excess pore pressure should be caused by the increase in wave height. In addition, the maximum increase in transient excess pore pressure is approximately 8 kPa, and considering the effective stress at this depth range, this increase is small.

Table 4 The ratio of \bar{P}_e/σ_0' in each layer

Time	\bar{p}_e/σ_0' (%)							
	0.8 m	1.3 m	1.8 m	2.3 m	2.8 m	3.3 m	3.8 m	4.8 m
8:19	12.5	8.0	7.9	4.7	1.7	1.5	3.4	2.6
8:59	54.9	30.1	17.7	8.7	2.8	0.3	3.7	2.8
9:09	67.8	64.1	49.0	29.9	13.0	5.1	4.0	3.0
9:19	80.9	79.2	63.0	46.5	28.5	14.2	3.5	2.7
9:29	89.5	93.0	84.6	82.8	79.3	53.1	2.4	2.4
9:39	91.9	97.4	92.8	93.7	91.1	69.2	2.5	2.3
9:49	72.7	107.7	108.7	106.9	105.7	93.0	1.8	3.3
9:59	51.6	110.6	114.2	109.1	107.5	105.8	3.0	4.2
10:09	53.3	88.6	117.3	112.2	108.1	109.2	2.4	4.1
10:19	103.4	81.6	119.9	111.5	111.6	108.4	1.7	2.4
10:29	100.8	109.8	121.1	115.5	113.1	106.1	1.1	2.2

Due to the missing data from 8:29 to 8:49, the time when the excess pore pressure is first induced cannot be determined by the collected data directly. However, it was easily determined that there was no excess pore pressure before 8:19.

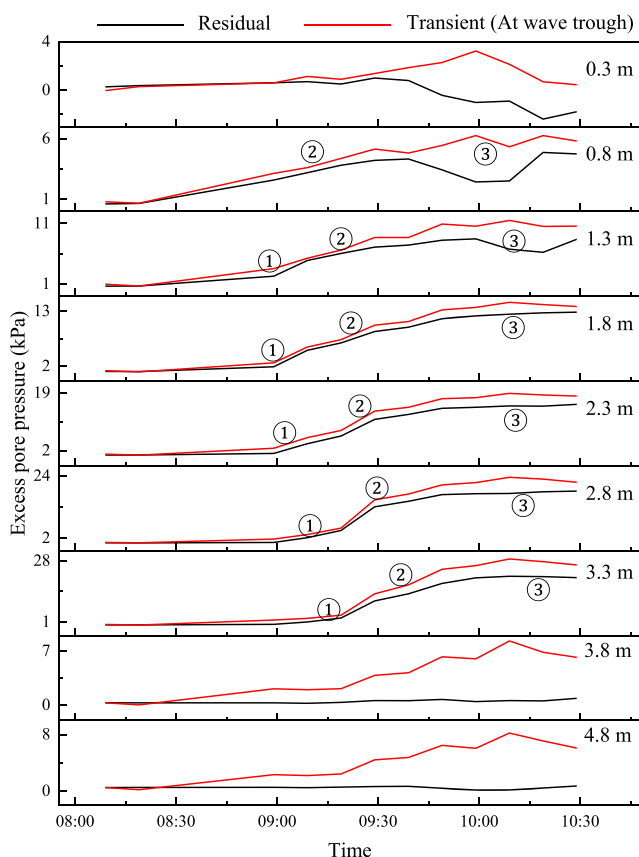


Fig. 12 Time-history curve of excess pore pressure during wave height increase

Liquefaction identification

The excess pore pressure from the seabed surface to a depth of 3.3 m peaks under waves with $H_{max} = 3.32$ m at approximately 10:00. Although the wave height continues to increase before 13:50, when H_{max} reaches 4.66 m, the excess pore pressure no longer increases. The excess pore pressure recorded in the soil onsite rapidly increases from shallow to deep under cyclic loading and then gradually decreases to a normal level from deep to shallow. This phenomenon is consistent with the response of the excess pore pressure before and after soil liquefaction observed in laboratory experiments (Sumer et al. 1999; Sumer et al. 2006a).

Theoretically, soil will liquefy only when the excess pore pressure is equal to the initial effective stress, that is, when the effective stress drops to 0. However, according to experimental research, it is found that when liquefaction occurs, the effective stress does not necessarily drop to 0 but is related to the clay content: within a certain range, the higher the clay content is, the lower the effective stress reduction ratio (Xu et al. 2012). Because the site soil is mainly silty soil, which implies a certain clay content, liquefaction may occur even if P_e/σ_{v0}' in a certain layer does not reach 100%. According to the change in P_e/σ_{v0}' (Fig. 11; Table 3), the maximum value of P_e/σ_{v0}' reaches 93% or higher from 0 to 3.3 m and 22.3% at 3.8 m or deeper. Another identification condition of seabed liquefaction \bar{P}_e/σ_0' increases to more than 100% after 9:40 from 1.3 to 3.3 m and remains at approximately 0 at 3.8 m or deeper (Fig. 11; Table 4). Based on the changes in excess pore pressure and the effective soil stress, the seabed is liquefied under the action of waves, and the liquefaction depth is between 3.3 and 3.8 m.

In addition, according to wave flume experiments, there is a layer of high-concentration suspended sand over the liquefied soil. Both oscillate with the overlying water under wave

action, but unlike the elliptical orbit of the water and liquefied soil, the orbit of the suspended sand is semielliptical (Wang 2010). This may cause the pore pressure to behave differently from the soil and water column. If sensors no. 7 and no. 8 are in this layer, this phenomenon may lead to their irregular response to wave action (Figs. 7 and 8), which indicates that the liquefaction depth is at least 1.3 m at 9:49.

Analysis of liquefaction depth development

Under the action of cyclic wave loading, the excess pore pressure in soil continuously increases, and the effective soil stress gradually decreases until the soil liquefies. According to the definition of liquefaction, it is also generally accepted that soil liquefaction occurs when \bar{P}_e/σ_0' reaches 100%. However, the field data are not continuous, and the wave condition is not stable, which leads to an irregular change in excess pore pressure; thus, it is impossible to accurately determine the liquefaction time of each layer. Through data fitting, the excess pore pressure at each time can be inferred, and then the liquefaction time of each layer can be inferred. The corresponding results are shown in Fig. 13.

As shown in Fig. 13, the time when the fitting line of \bar{P}_e/σ_0' reaches 100% can be regarded as the liquefaction time at that depth (Table 5). Since \bar{P}_e/σ_0' does not reach 100% at a depth of 0.8 m, it is not shown in Fig. 13. Although the liquefaction time at this depth cannot be determined by the method

Table 5 Liquefaction time of each layer

Depth (m)	Δz (m)	Liquefaction time	Δt (min)	v (m/min)
1.3		9:40:07		
1.8	0.5	9:42:40	2.55	0.20
2.3	0.5	9:43:35	0.92	0.54
2.8	0.5	9:45:03	1.47	0.34
3.3	0.5	9:54:51	9.81	0.05
Total	2.0	–	14.74	0.17

mentioned above, it can be inferred that the soil at 0.8 m is liquefied before that at 1.3 m.

According to the liquefaction time of each layer based on the fitted line, the soil is gradually liquefied from shallow to deep within the range of 1.3–3.3 m, which means that the silty soil seabed liquefaction develops in a top-down manner under wave action. At the same time, the downward development rate of the liquefaction depth is not uniform. One of the reasons for this pattern may be the irregularity of the waves. Due to the discontinuity of the data, not all the waves at the monitoring point are recorded, but according to the monitored data, the change in wave height will lead to a change in the liquefaction rate. Another factor influencing the liquefaction rate is the non-homogeneity of the seabed soil along the vertical direction. The attenuation of wave action caused by the seabed depth (Fig. 7) may also be a factor. According to laboratory test records (Kirca 2013; Ren et al. 2020), even if the wave height remains constant, the rate of liquefaction development will gradually decrease with increasing depth. These factors explain the phenomenon of the slower liquefaction rate of the deeper layer (2.8–3.3 m) at higher wave heights compared with the liquefaction rate of the shallower layer (1.3–2.8 m) at lower wave heights.

If the inhomogeneity of soil liquefaction depth development is ignored, the liquefaction depth develops from 1.3 to 3.3 m within 14.74 min, i.e., the average top-down development rate of the soil liquefaction depth is 0.17 m/min.

Conclusions

To study the problem of liquefaction of a silty soil seabed under the action of waves, the pore pressure responses under waves in a seabed at a water depth of 8.4 m were monitored in the Chengdao area, Yellow River delta. According to the pore pressure data obtained on 5 November 2015, the findings may be summarized as follows:

1. The seabed starts to liquefy under waves with $H_{1/3} = 0.5$ m and $T_{1/3} = 6.53$ s in the Yellow River delta.
2. Silty soil seabed liquefaction develops in a top-down manner under wave action.

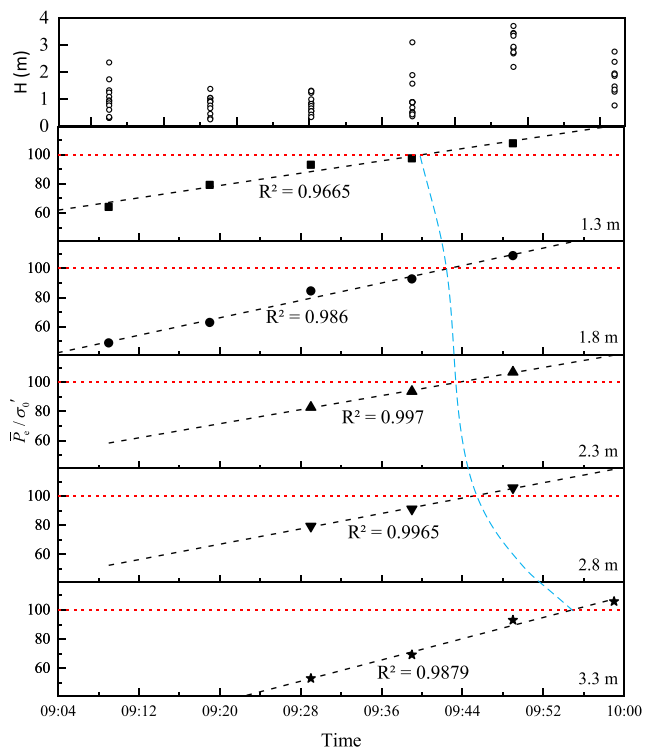


Fig. 13 Monitoring values and fitting curves of \bar{P}_e/σ_0' at each layer

3. Under the action of waves with $H_{1/3} = 3.65$ m and $T_{1/3} = 9.78$ s, the liquefaction depth is between 3.3 and 3.8 m.
4. Under field conditions of the monitoring point, the average top-down development rate of the liquefaction depth is approximately 0.17 m/min.

Funding This study was funded by the National Natural Science Foundation of China (Grant No. 41576039).

Abbreviations d , grain size; h , water depth; H , wave height; \bar{H} , average wave height; H_{\max} , maximum wave height; $H_{1/3}$, significant wave height; K , coefficient of permeability; K_p , pressure coefficient; k_0 , lateral earth pressure coefficient at rest; P , magnitude of the pressure change at the water bottom; P_e , excess pore pressure; \bar{P}_e , residual excess pore pressure; P_m , measured pore pressure; P_z , magnitude of the pressure change at burial depth z ; P_0 , static pore pressure; T , wave period; \bar{T} , average wave period; $T_{1/3}$, significant wave period; v , development rate of liquefaction depth; W_g , water content; z , burial depth of the sensor; γ , unit weight; γ_s , effective unit weight of soil; γ_w , effective unit weight of sea water; σ , effective stress; σ_{v0} , initial vertical effective stress; σ'_0 , initial effective stress

References

- Bennett RH (1977) Pore-water pressure measurements: Mississippi delta submarine sediments. *Mar Geotechnol* 2:177–189
- Bennett RH, Faris JR (1979) Ambient and dynamic pore pressures in fine-grained submarine sediments: Mississippi Delta. *Appl Ocean Res* 1:115–123
- Bornhold BD, Yang Z, Keller GH, Prior DB, Wiseman WJ, Wang Q, Wright LD, Xu W, Zhuang Z (1986) Sedimentary framework of the modern Huanghe (Yellow River) delta. *Geo-Mar Lett* 6:77–83
- Cha D, Zhang H, Blumenstein M (2011) Prediction of maximum wave-induced liquefaction in porous seabed using multi-artificial neural network model. *Ocean Eng* 38:878–887
- Chen W, Yang Z, Prior DB (1992) The classification and analysis of seafloor micromorphology on the Huanghe (Yellow River) subaqueous slope. *J Ocean Univ Qingdao* 22:71–81
- Christian J, Taylor P, Yen J, Erali D (1974) Large diameter underwater pipeline for nuclear power plant designed against soil liquefaction. Proc. 6th Offshore Tech. Conf., Dallas. pp. 597–606
- Dalrymple RA, Liu PL (1978) Waves over soft muds: a two-layer fluid model. *J Phys Oceanogr* 8:1121–1131
- Davis EE, Horel GC, Macdonald RD, Villinger H, Bennett RH, Li H (1991) Pore pressures and permeabilities measured in marine sediments with a tethered probe. *J Geophys Res-Sol Ea* 96:5975–5984
- Gagniere S, Smith SGL, Yeh HD (2018) Excess pore water pressure due to ground surface erosion. *Appl Math Model* 61:72–82
- Kirca VSO (2013) Sinking of irregular shape blocks into marine seabed under wave-induced liquefaction. *Coast Eng* 75:40–51
- Kirca VSO, Sumer BM, Fredsøe J (2013) Residual liquefaction of seabed under standing waves. *J Waterw Port Coast* 139:489–501
- Liu Z, Jeng D, Chan AHC, Luan M (2010) Wave-induced progressive liquefaction in a poro-elastoplastic seabed: a two-layered model. *Int J Numer Anal Met* 33:591–610
- Miyamoto J, Sassa S, Sekiguchi H (2004) Progressive solidification of a liquefied sand layer during continued wave loading. *Géotechnique* 54:617–629
- Mory M, Michallet H, Bonjean D, Piedra-Cueva I, Barnoud JM, Foray P, Abadie S, Breul P (2007) A field study of momentary liquefaction caused by waves around a coastal structure. *J Waterw Port Coast* 133:28–38
- Prior DB, Yang ZS, Bornhold BD, Keller GH, Lu NZ, Wiseman WJ, Wright LD, Zhang J (1986) Active slope failure, sediment collapse, and silt flows on the modern subaqueous Huanghe (Yellow River) delta. *Geo-Mar Lett* 6:85–95
- Prior DB, Suhayda JN, Lu N, Bornhold BD, Keller GH, Wiseman WJ, Wright LD, Yang Z (1989) Storm wave reactivation of a submarine landslide. *Nature* 341:47–50
- Puzrin AM, Alonso EE, Pinyol NM (2010) Caisson failure induced by liquefaction: Barcelona Harbour, Spain. In: *Geomechanics of Failures*. Springer, Dordrecht, pp 85–148
- Qi W, Gao F (2018) Wave induced instantaneously-liquefied soil depth in a non-cohesive seabed. *Ocean Eng* 153:412–423
- Ren Y, Xu G, Xu X, Zhao T, Wang X (2020) The initial wave induced failure of silty seabed: liquefaction or shear failure. *Ocean Eng* 200:106990
- Richards AF, Øten K, Keller GH, Lai JY (1975) Differential piezometer probe for an in situ measurement of sea-floor. *Géotechnique* 25: 229–238
- Sassa S, Sekiguchi H (1999) Wave-induced liquefaction of beds of sand in a centrifuge. *Géotechnique* 49:621–638
- Sassa S, Takayama T, Mizutani M, Tsujio D (2006) Field observations of the build-up and dissipation of residual pore water pressures in seabed sands under the passage of storm waves. *J Coast Res* 39:410–414
- Sumer BM (2014) Liquefaction around marine structures. World Scientific, Singapore
- Sumer BM, Fredsøe J, Christensen S, Lind MT (1999) Sinking/floatation of pipelines and other objects in liquefied soil under waves. *Coast Eng* 38:53–90
- Sumer BM, Hatipoglu F, Fredsøe J, Sumer SK (2006a) The sequence of sediment behaviour during wave-induced liquefaction. *Sedimentology* 53:611–629
- Sumer BM, Truelsen C, Fredsøe J (2006b) Liquefaction around pipelines under waves. *J Waterw Port Coast* 132:266–275
- Wang X (2010) Experimental study on movement characteristics of liquefied silty seabed under waves. Dissertation, Ocean University of China
- Wang G, Xu G, Liu Z, Liu H, Sun Z (2017) Experimental study of the physical and mechanical characteristics changes of wave-induced liquefied silt. *Mar Geol Quat Geol* 37:176–183
- Williams S, Arsenault MA, Buczkowski BJ, Reid JA, Flocks J, Kulp MA, Penland S, Jenkins CJ (2006) Surficial sediment character of the Louisiana offshore continental shelf region: a GIS compilation. U.S. Geological Survey Open-File Report. 2006–1195. Online at (<http://pubs.usgs.gov/of/2006/1195/index.htm>)
- Xu G, Sun Y, Wang X, Hu G, Song Y (2009) Wave-induced shallow slides and their features on the subaqueous Yellow River delta. *Can Geotech J* 46:1406–1417
- Xu G, Liu H, Liu J, Yu Y (2012) Role of clay content in silty soil liquefaction. *Mar Geol Quat Geol* 32:31–35
- Xu G, Liu Z, Sun Y, Wang X, Lin L, Ren Y (2016a) Experimental characterization of storm liquefaction deposits sequences. *Mar Geol* 382:191–199
- Xu G, Wang G, Lv C, Sun Z (2016b) Experimental study on the motion forms of outflowed sediments from wave-induced liquefied seabed. *Period Ocean Univers China* 46:98–105
- Zen K, Yamazaki H (1990a) Mechanism of wave-induced liquefaction and densification in seabed. *Soils Found* 30:90–104
- Zen K, Yamazaki H (1990b) Oscillatory pore pressure and liquefaction in seabed induced by ocean waves. *Soils Found* 30:147–161
- Zen K, Yamazaki H (1991) Field observation and analysis of wave-induced liquefaction in seabed. *Soils Found* 31:161–179

Publisher's note Springer Nature remains neutral with regard to jurisdictional claims in published maps and institutional affiliations.